AiMT

Advances in Military Technology
Vol. 14, No. 1 **(2019)**, pp. 151-161
ISSN 1802-2308, eISSN 2533-4123
DOI 10.3849/aimt.01268

Analysis of Impact of Conic Aperture in Differentially Pumped Chamber

J. Maxa*, P. Hlavatá and P. Vyroubal

Department of Electrical and Electronic Technology, Faculty of Electrical Engineering and Communication, Brno University of Technology, Czech Republic

The manuscript was received on 6 September 2018 and was accepted after revision for publication on 15 June 2019

Abstract:

The paper focuses on the simulation of medium dynamics in the environmental scanning electron microscope. In particular, the paper examines the conical aperture location effect in the differentially pumped chamber and the width of the pumping channel in this chamber. The solution is based on the Taylor-Maccoll theory about the impact of the shock wave and was obtained by the use of continuum and finite volume methods in the ANSYS Fluent system.

Keywords:

ANSYS Fluent, differentially pumped chamber, environmental scanning electron microscope (ESEM), finite volume method, Taylor-Maccoll theory

1. Introduction

The present paper follows the work by Danilatos [1], which deals with the problem of the shape impact of the differentially pumped chamber of the electron microscope on the pressure field in the given chamber. Fig. 1 shows the identical axis of the chamber with the primary path of the electron beam. The pressure value, achieved in the axis of the differentially pumped chamber, in which the primary electron beam goes through, is the first main criterion [2, 3]. The second main criterion is the mass flow rate through the aperture PLA 2 towards the tube [1, 4].

In the microscope (ESEM), the differentially pumped chamber with the aperture PLA 1 (Fig. 2) separates the area of the specimen chamber in which a high value of pressure is maintained (up to 2000 Pa) and the aperture PLA 2 separates the area of the tube (0.01 Pa) [5]. The requirement for the differentially pumped chamber during its operation – while interacting with the gas molecules during their passage through the

* *Corresponding author: Department of Electrical and Electronic Technology, Faculty of Electrical Engineering and Communication, Brno University of Technology, Czech Republic. Phone: +420 54114 6129, fax: +420 54114 6129, E-mail: maxa@feec.vutbr.cz*

chamber – is to have the least dispersed electron beam, because its dispersion causes reduced sharpness up to the total destruction of the resulting image [6].
During construction of the differentially pumped chamber, the following requirements are to be met:

- to ensure the least electron dispersion in the primary beam axis [7],
- to ensure the least mass flow rate towards the tube through the aperture PLA 2 [8].

Fig. 1 shows the gas density field given trough the Normalized Density Number.

The number of atoms or molecules (n) in a mass (m) of a pure material having atomic or molecular weight (M) is easily computed from the following equation using Avogadro number (N_A):

$$n = \frac{mN_A}{M}. \tag{1}$$

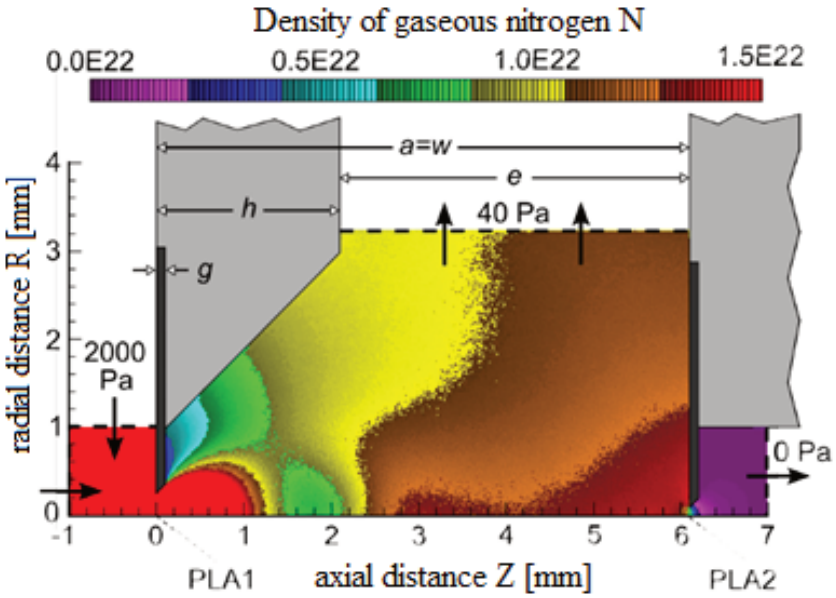

Fig. 1 Primary electron beam path between the apertures [1]

In case the density ρ of the substance is given, the atomic number density N, which is the concentration of atoms or molecules per unit volume V, becomes a more convenient quantity to compute. It can be found as

$$N = \frac{n}{V} = \frac{\rho N_A}{M}, \quad [\mathrm{m}^{-3}]. \tag{2}$$

The original field of the Normalized Density Number is shown in Fig. 1. Here, the microscope axis is shown by axial distance Z, which is also the primary path of the electron beam between the apertures PLA 1 and PLA 2 within the range from 0 mm to 6 mm [1].

2. Adjustment of Aperture PLA 2

The improved design of the differentially pumped chamber is based on the change of the PLA 2 aperture shape. It was designed as a conical aperture and the cone was extended and placed into the supersonic flow area. Such a shape of the aperture protects the area with a significant density increase, which was created by the flat aperture. The modified conical aperture PLA 2 is shown in Fig. 2 [1].

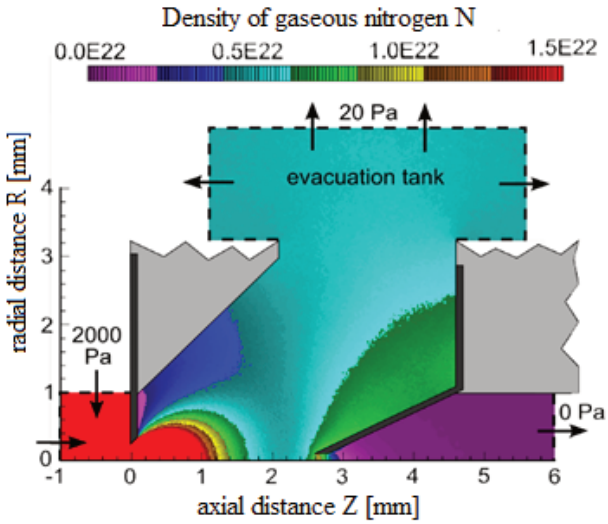

Fig. 2 Use of conical aperture PLA 2 for appropriate experimentally obtained conditions [1]

This study concerns the impact of the conical aperture (PLA 2) shape change and the impact of the mid-aperture distance on the formation of shock waves. In addition, the Taylor-Maccoll theory was used to determine a final shape of the shock wave which is formed behind the conical aperture. The effect of the pressure loss along the path of an oblique shock wave on the mass flow into the tube was studied as well.

3. Taylor-Maccoll Analysis

Due to the pressure ratios, the flow behind the outlet of the aperture PLA 1 is supersonic. In the design of the aperture PLA 2, it is necessary to take into account the angle of the aperture cone PLA 2 which has an impact on the character of the shock wave emerging in front of this cone. In the supersonic regime (Ma > 1), a shock wave is created in front of the head of the aperture cone PLA 2.

Depending on the value of the Mach number and the value of the cone angle, two basic shapes of the shock wave can take place: either an oblique shock wave or a detached shock wave (Figs 3, 4). It is important to mention here that the oblique shock wave does not cause as big pressure loss as the detached shock wave does [9].

Using an appropriate value of the cone angle, it is necessary to endeavor achieving an oblique shock wave, because of a favorable flow character through the aperture PLA 2.

The Taylor-Maccoll procedure of the flow calculation consists of four steps:

- for the given values of the Mach number and cone angles, guess a shock angle and use the oblique shock relations to determine velocity V downstream of shock. Resolve into V_r (radial) and V_θ (angular),
- numerically integrate the Taylor-Maccoll differential equations for V_r and V_θ (Eqs (3) and (4)) from the shock wave until $V_\theta = 0$,

$$\frac{\gamma-1}{2}\left[1-V_r^2-\left(\frac{dV_r}{d\theta}\right)^2\right]\left[2V_r+\cot\theta\frac{dV_r}{d\theta}+\frac{d^2V_r}{d\theta^2}\right]-\frac{dV_r}{d\theta}\left[V_r\frac{dV_r}{d\theta}+\frac{dV_r}{d\theta}\frac{d^2V_r}{d\theta^2}\right]=0\,, \quad (3)$$

$$V_\theta=\frac{dV_r}{d\theta}\,. \quad (4)$$

- $V_\theta = 0$ at $\theta = \theta_{surf}$. Adjust the shock angle and repeat the process until θ_{surf} = cone angle,
- use isentropic relations to determine the flow variables along each ray.

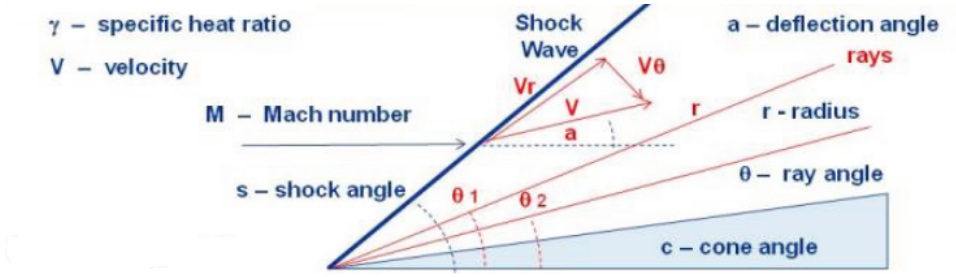

Fig. 3 Ratio of the flow velocity and the cone angle[1]

Fig. 4 shows the dependence of the limiting cone angle on the Mach number [9]. In the area above the curve, the detached shock wave is formed, while the oblique shock wave is formed below the curve.

The information shown in Fig. 4 was used for choosing the shape of the conical aperture PLA 2, the evaluation of the angle of the conical aperture and its location in the supersonic flow. It is worth noting here that the pressure loss originates behind the detached shock wave, which, in the given case, favorably affects the reduced flow to the aperture PLA 2.

4. Aperture PLA 2 Versions

Two values of the conical aperture PLA 2 angle were chosen – 17° (Fig. 5 left) and 37° (Fig. 5 right) – to evaluate how the shape and location of the mentioned aperture affect the dispersion of the primary electron beam and mass flow rate to the tube through that aperture. Both versions were analyzed for four different spacings between the apertures PLA 1 and PLA 2, namely: 1.1 mm, 2.1 mm, 3.1 m, and 4.1 mm (marked as X on Fig. 5).

Overall, eight models were evaluated which differed by the distance between the apertures PLA 1 and PLA 2 and by the angle of the aperture PLA 2. These versions are

[1] https://www.grc.nasa.gov/WWW/k-12/airplane/coneflow.html

listed in Tab. 1. Each version is characterized by the distance between the apertures and the cone angle.

A numerical solution was obtained by the use of continuum and finite volume methods in the ANSYS Fluent system. Because a supersonic flow is considered, the density base model with the second order discretization was chosen.

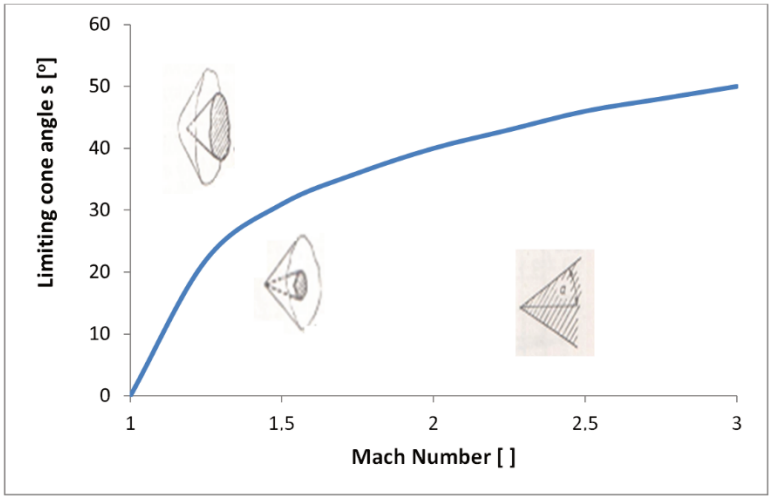

Fig. 4 Dependence of the cone angle on Mach number [9]

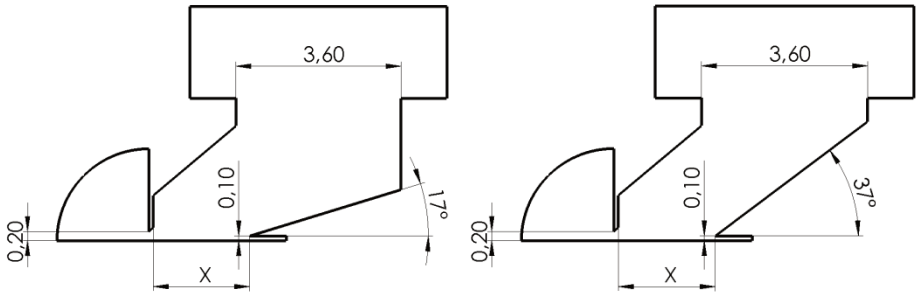

Fig. 5 Angle adjustment of aperture PLA 2

Tab. 1 Models versions

Version	1.1-17	1.1-37	2.1-17	2.1-37	3.1-17	3.1-37	4.1-17	4.1-37
Distance *x* [mm]	1.1	1.1	2.1	2.1	3.1	3.1	4.1	4.1
Angle [°]	17	37	17	37	17	37	17	37

5. Results

For each model, five basic quantities were evaluated, namely: the gas flow velocity, the normalized density number, the temperature, the pressure in the differentially pumped chamber, and the mass flow from the aperture PLA 2 to the tube. An expected probability of the electron dispersion was evaluated from the data about the flow along the primary beam path.

Fig. 6 shows the dependence of the gas flow velocity on the distance between the PLA 1 and PLA 2. From the figure, it is obvious that the gas flow velocity decreases as the distance from PLA 1 increases, whereas the model of 1.1 mm produces the lowest flow velocity of 100 m s^{-1} and the model with the longest distance of 4.1 mm and angle of 17° decreases that velocity up to the value of 28 m s^{-1}.

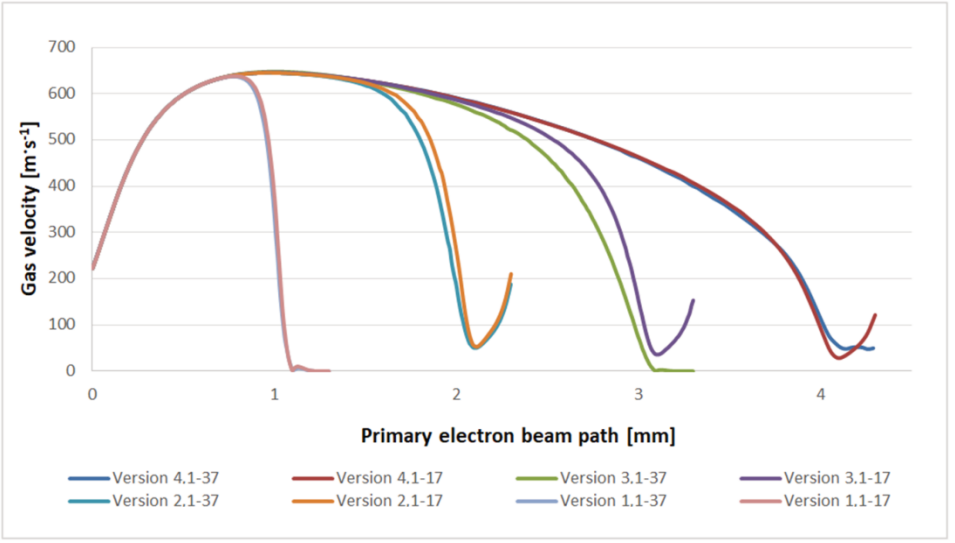

Fig. 6 Graphic of dependence of gas flow velocity on distance from PLA 1

In the models with the aperture distance of 1.1 mm, 2.1 mm, and 3.1 mm, the aperture PLA 2 intrudes into the area of the supersonic flow. This is why the flow braking is more intensive than in the model of 4.1 mm.

The velocity gradient is also distinct for each of the models, from its highest value to the lowest one. The models with the distance of 1.1 mm produce the highest gradient values.

The velocity increase at the end of the curves is caused by the re-accelerating flow which occurs in the aperture PLA 2.

Fig. 7 shows the gas particle density over the distance from the aperture PLA 1 in the direction to PLA 2. The highest gas density in front of the aperture PLA 2 inlet comes out in the model with the apertures distance of 1.1 mm, where the gas has the highest density after the passage through the aperture PLA 1, because of the significant gas braking from the high speed. This also applies to the model with the aperture PLA 2 angle of 17° and 37°. In other models, the braking from a high speed does not occur. From the figure it is obvious that the gas density declines with the increasing apertures distance.

In front of the inlet of the aperture PLA 2, the gas braking occurs, thus, the density increases. The faster the braking, the higher the density, therefore, the density increase within the distance between the apertures PLA 1 and PLA 2 declines.

Fig. 8 shows the temperature dependence on the distance from PLA 1, the temperature is within the interval from −50 °C to −180 °C. The reason for the fast gas temperature reduction is the supersonic flow. Due to this reason, all models have similar temperature behavior up to its minimum. Upon reaching its minimum, the temperature

begins to rise and with the increased distance between the apertures the temperature changes slowly.

The pressure dependence on the distance from PLA 1 is shown in Fig. 9. As in case of the gas particle density, the model with the aperture distance of 1.1 mm is the most different, that is, it develops the largest pressure rise in front of PLA 2.

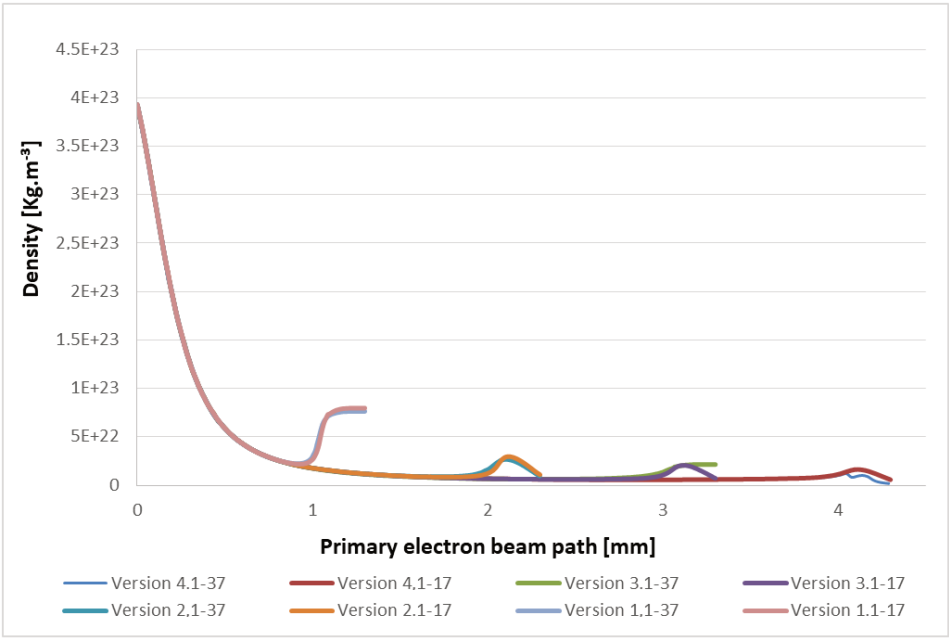

Fig. 7 Graphic of gas density dependence on distance PLA 1

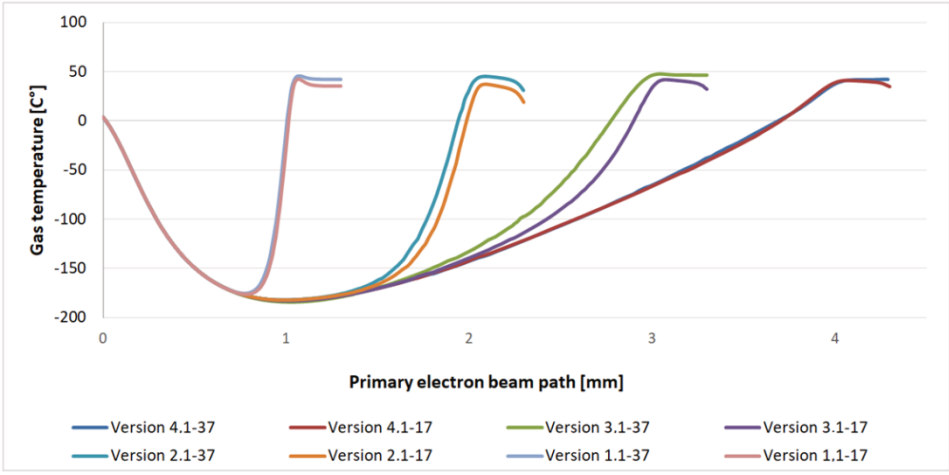

Fig. 8 Graphic of temperature dependence on distance from PLA 1

The one main criterion - the probability of the electron dispersion, is derived from the given pressure running on the primary electron beam path. The electron is directly proportional to the product of the pressure values and the distance which an electron

runs. Due to the significant initial dependence of the pressure on the distance offsets by an electron from the PLA 2 up to PLA 1 (quantity d) can be expressed using integral:

$$P_{\mathrm{d}} = \int p(x)\mathrm{d}x \,. \tag{5}$$

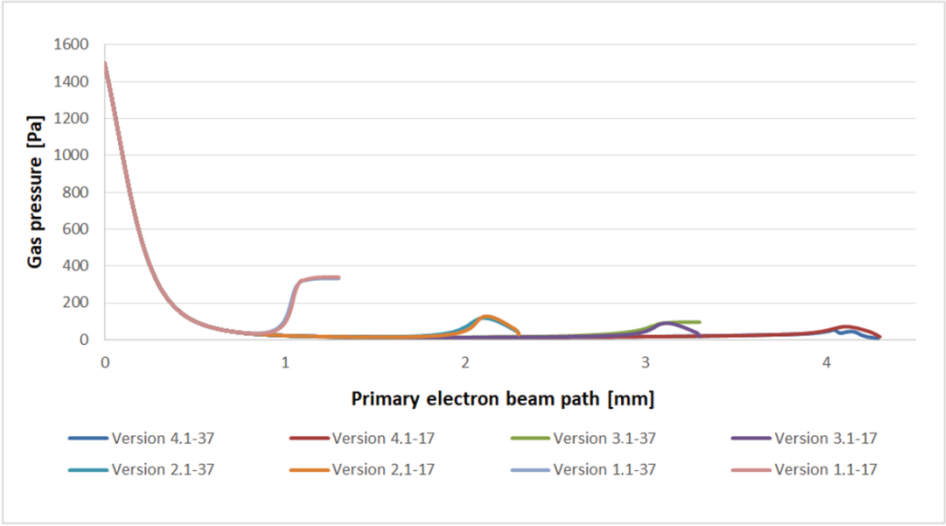

Fig. 9 Graphic of pressure dependence on distance from PLA 1

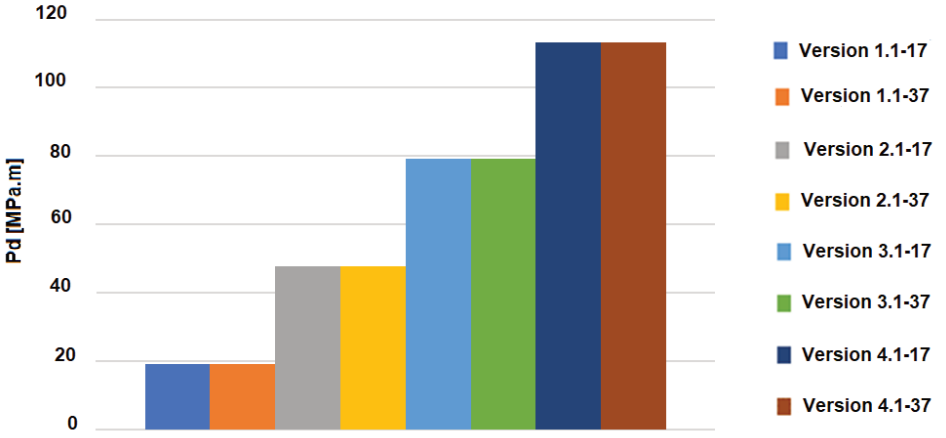

Fig. 10 Graphic of probability of electron dispersion of each version

From the values of the electron dispersion shown it is obvious that, as the distance between the apertures PLA increases, the probability of the electron dispersion also increases. This brings a negative effect in the form of a smaller amount of the impinging electrons on the tested element and overall image deterioration. That is why it is desirable to keep the dispersion as little as possible.

The second criterion is the mass flow rate through the aperture PLA 2 to the tube, which is shown in Fig. 11 for all models. In case of a large value of the mass flow rate, one is unable to maintain vacuum in the tube and the microscope would lose its function.

From the presented data, it follows that the mass flow rate of the gas in the direction towards the aperture PLA 2 decreases as the distance between the apertures PLA 1 and PLA 2 increases. It comes out that, for all the models, a bigger angle delivers a better result due to the detached shock wave, behind which a bigger pressure loss occurs [10-12]. The difference in the character of the shock wave being formed behind the aperture PLA 2 becomes obvious from Fig. 12, which shows the iso-surface of the Mach number with the angle of 17° (Fig. 12, left) and with the angle of 37° (Fig. 12, right). The angle of 17° exhibits a more oblique character of the Mach number isosurface.

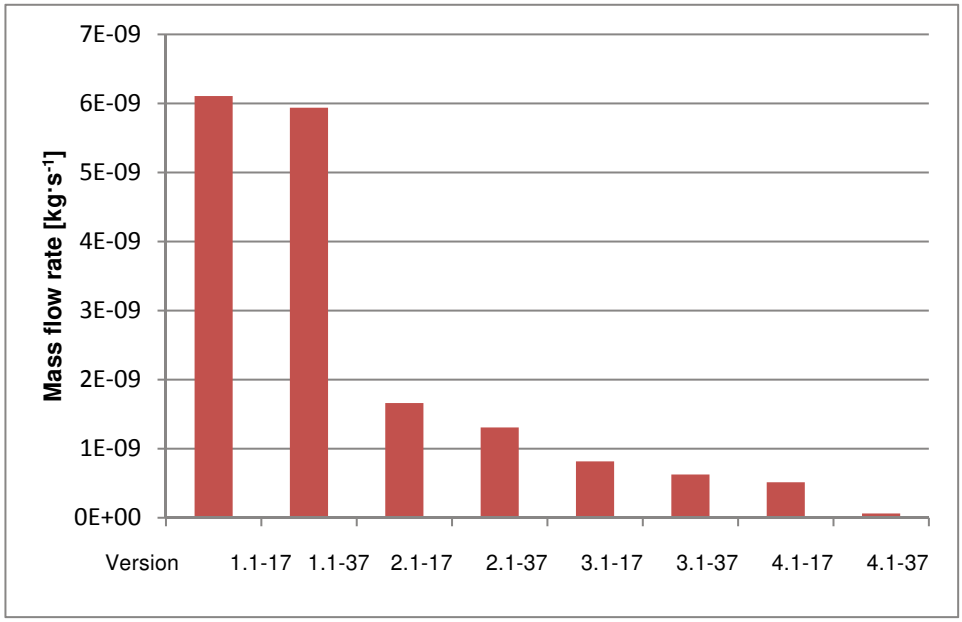

Fig. 11 Evaluation of mass flow rate through aperture PLA 2

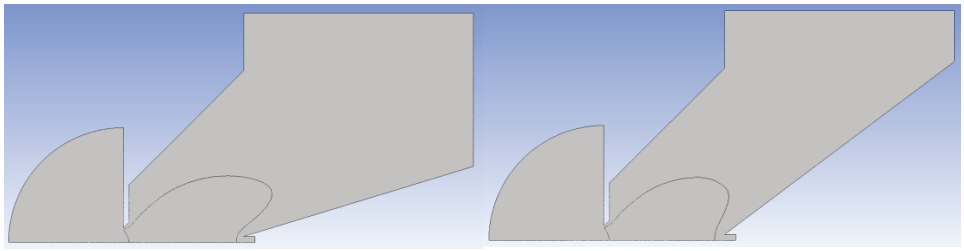

Fig. 12 Iso-surface of Mach number for both angle versions

6. Conclusions

From the results presented in this study, it follows that, as far as the first criterion is concerned, the version with the distance of 1.1 mm between the apertures delivers the least probability of the electron dispersion.

At the same time, as far as the second criterion is concerned, the version with the aperture distance of 4.1 mm and angle of 37° provides the best mass flow rate in the aperture PLA 2.

Since two different versions deliver the best results as far as the two criteria are concerned, the version with the distance of 2.1 mm with the angle of 37° has been chosen as a compromise between the two. This is because none of the two criteria can be compromised.

This version will be used for the modernization of the actual version of the environmental electron scanning microscope, whereas the sharpness of the image will be experimentally verified.

To maintain a high level of defense, the usage of electron microscopy is absolutely necessary in the military technology. This is also due to a wide range of possibilities such a usage offers. One of the examples is the invention of a lightweight plastic with the strength of steel for construction of a light armor, which absorbs projectile energy well. This would not be possible without using an electron microscope.

Suffice it to say that the electron microscope Mini SEM was designed solely for the purposes of the army in terrain.

Similarly, such army components as USAMRIID (United States Army Medical Research Institute of Infectious Diseases) would not be able to perform without electron microscopy. Among the success stories of the USAMRIID is using self-vaccine against the Venezuelan equine encephalitis in 1971, which allowed to confine the epidemic in the South of the United States.

Based on the above mentioned facts, electron microscopy is indispensable for the army, in particular, for the Research Analytical Laboratory at the Department of Mechanical Engineering equipped with the top quality diagnostic technique and the electron microscope Tescan VEGA 5135.

Acknowledgement

We would like to thank to Ing. et. Ing. Vilém Neděla, Ph.D. from the Institute of Scientific Instruments of the Czech Academy of Sciences in Brno for consultations in given issues. Publication was supported by the internal grant FEKT-S-14-2293 (Materials and technology for electrical engineering II).

References

[1] DANILATOS, G. Velocity and Ejector-jet Assisted Differential Pumping: Novel Design Stages for Environmental SEM. *Micron*, 2011, vol. 43, no. 5, p. 600-611. DOI 10.1016/j.micron.2011.10.023.

[2] VYROUBAL, P., MAXA, J., NEDĚLA, V., JIRÁK, J. and HLADKÁ, K. Apertures with Laval Nozzle and Circular Orifice in Secondary Electron Detector for Environmental Scanning Electron Microscope. *Advances in Military Technology*. 2013, vol. 8, no. 1, p. 59-69. ISSN 1802-2308.

[3] MAXA, J. and NEDĚLA, V. The Impact of Critical Flow on the Primary Electron Beam Passage through Differentially Pumped Chamber. *Advances in Military Technology,* 2011, vol. 6, no. 1, p. 39-46. ISSN 1802-2308.

[4] NEDĚLA, V., TIHLAŘÍKOVÁ, E., RUNŠTUK, V. and HUDEC, J. High-Efficiency Detector of Secondary and Backscattered Electrons for Low-Dose Imaging in the ESEM. *Ultramicroscopy*, 2018, 184 (Pt A), p. 1-11. DOI 10.1016/j.ultramic.2017.08.003.

[5] NEDĚLA, V., KONVALINA, I., ORAL, M. and HUDEC, J. The Simulation of Energy Distribution of Electrons Detected by Segmental Ionization Detector in High Pressure Conditions of ESEM. *Microscopy and Microanalysis*, 2015, vol. 21, no. 54, p. 264-269. DOI 10.1017/S1431927615013483.

[6] NEDĚLA, V., HŘIB, J., HAVEL, L., HUDEC, J. and RUNŠTUK, J. Imaging of Norway Spruce Early Somatic Embryos with the ESEM, Cryo-SEM and Laser Scanning Microscope. *Micron*, 2016, vol. 84, p. 67-71. DOI 10.1016/j.micron.2016.02.011.

[7] MAXA, J., BÍLEK, M., HLAVATÁ, P., VYROUBAL, P. and LEPLTOVÁ, K. Comparisons Using Methods of Continuum Mechanics and Monte Carlo at Differentially Pumped Chamber. *Advances in Military Technology*, 2016, vol. 11, no. 2, p. 143-150. ISSN 1802-2308.

[8] MAXA, J., NEDĚLA, V., JIRÁK, J., VYROUBAL, P. and HLADKÁ, K. Analysis of Gas Flow in a Secondary Electron Scintillation Detector for ESEM with a New System of Pressure Limiting Apertures. *Advances in Military Technology*, 2012, vol. 7, no. 2, p. 39-44. ISSN 1802-2308.

[9] DANĚK, M. *Aerodynamics and Flight Mechanics* (in Czech). Brno: Akademické nakladatelství CERM, 2009. 293 p. ISBN 978-80-7204-659-1.

[10] HLAVATÁ, P., MAXA, J., BÍLEK, M., LEPLTOVÁ, K. and BAYER, R. Influence of Critical Flow in the Differentially Pumped Chamber AQUASEM. *Advances in Military Technology,* 2017, vol. 12, no. 2, p. 301-310. ISSN 1802-2308. DOI 10.3849/aimt.01201.

[11] HLAVATÁ, P., MAXA, J., BÍLEK, M. and NEDĚLA, V. Impact of the Shape of the Differentially Pumped Chamber on Critical Flow Character. *ECS Transaction,* 2017, vol. 81, no. 1, p. 317-322. DOI 10.1149/08101.0317ecst.

[12] BÍLEK, M., MAXA, J., HLAVATÁ, P. and BAYER, R. Modelling and Simulation of a Velocity Field Within Supersonic Flow in Low-Pressure Areas. *ECS Transaction,* 2017, vol. 81, no. 1, p. 311-316. DOI 10.1149/08101.0311ecst.